

# Determination of Superconducting Parameters of $\text{GdBa}_2\text{Cu}_3\text{O}_{7-\delta}$ Added with Nanosized Ferrite $\text{CoFe}_2\text{O}_4$ from Excess Conductivity Analysis

A.I. Abou Aly · N.H. Mohammed · R. Awad ·  
H.A. Motaweh · D. El-Said Bakeer

Received: 5 April 2012 / Accepted: 7 May 2012 / Published online: 23 June 2012  
© Springer Science+Business Media, LLC 2012

**Abstract** Superconductor samples of the type  $(\text{CoFe}_2\text{O}_4)_x\text{GdBa}_2\text{Cu}_3\text{O}_{7-\delta}$ ,  $0.0 \leq x \leq 0.1$  wt.%, were synthesized by the conventional solid-state reaction technique and were characterized using X-ray powder diffraction (XRD) and scanning electron microscope (SEM). XRD analysis indicated that the orthorhombic structure of Gd-123 is not affected by nanosized ferrite  $\text{CoFe}_2\text{O}_4$  addition, whereas the volume fraction of Gd-123 increased up to  $x = 0.01$  wt.%. Excess conductivity analysis of the investigated samples was analyzed as a function of temperature using the Aslamazov and Larkin (AL) model. It exhibited four different fluctuation regions, namely critical (cr), three-dimensional (3D), two-dimensional (2D), and short-wave (sw). The zero-temperature coherence length along  $c$ -axis, effective layer thickness of the two-dimensional system, and inter-layer coupling strength were estimated as functions of nanosized ferrite  $\text{CoFe}_2\text{O}_4$  concentration. In addition, the thermodynamics, lower and upper critical magnetic fields, and critical current density were calculated from the Ginzburg number. It was found that the low concentration of nanosized ferrite  $\text{CoFe}_2\text{O}_4$  addition up to  $x = 0.01$  wt.% improved the physical properties of Gd-123, while for  $x > 0.01$  wt.%, these properties were deteriorated.

**Keywords** Gd-123 phase · Nanosized ferrite  $\text{CoFe}_2\text{O}_4$  · Excess conductivity · Critical magnetic fields

A.I. Abou Aly · N.H. Mohammed · R. Awad (✉)  
Physics Department, Faculty of Science, Alexandria University,  
Alexandria, Egypt  
e-mail: rawad64@yahoo.com

H.A. Motaweh · D. El-Said Bakeer  
Physics Department, Faculty of Science, Damanhur University,  
Damanhur, Egypt

## 1 Introduction

High-temperature superconductors  $R\text{Ba}_2\text{Cu}_3\text{O}_{7-\delta}$  ( $R = \text{Nd, Sm, Eu, and Gd}$ ) with an orthorhombic phase exhibit the superconducting transition temperature  $T_c$  around 90 K [1]. Its structure includes the typical  $\text{CuO}_2$  plane and the  $\text{Cu-O}$  chain like  $\text{YBa}_2\text{Cu}_3\text{O}_{7-\delta}$  (Y-123) phase. One of the promising phases for practical engineering applications in the  $R\text{Ba}_2\text{Cu}_3\text{O}_{7-\delta}$  families is  $\text{GdBa}_2\text{Cu}_3\text{O}_{7-\delta}$  since, in comparison with Y-123 [2], it possesses significantly better properties, such as high critical current density  $J_c$  [3], high ability to trap the magnetic field up to 3 T at 77 K [4], relative low crystalline anisotropy, and well-developed pinning properties in the magnetic field [5].

Recently, effect of nanosized additions inside bulk high-temperature superconductors (HTSCs) has been widely investigated [6–8]. A suitable amount of nanosized additions improve the microstructure and superconducting properties of these materials. This is due to the size of nanoparticles which is higher than the coherence length  $\xi$  and lower than the penetration depth  $\lambda$ , leading to strong interaction between flux line network and nanosized magnetic particles. The addition of nanosized  $\text{ZrO}_2$ ,  $\text{SnO}_2$ , and  $(\text{ZrO}_2+\text{ZnO})$  into bulk superconductor  $\text{GdBa}_2\text{Cu}_3\text{O}_{7-\delta}$  enhanced the flux pinning and consequently improved critical current density [9–11]. The effect of nanosized ferrite  $\text{CoFe}_2\text{O}_4$  on the physical properties of  $\text{YBa}_2\text{Cu}_3\text{O}_{7-\delta}$  thin film was reported by Wimbush et al. [12]. A reduction in  $J_c$  was observed as a result of  $\text{Y}(\text{Fe,Co})\text{O}_3$  formation instead of  $\text{CoFe}_2\text{O}_4$ . Kong et al. [13] investigated the effect of nanosized ferrite  $\text{NiFe}_2\text{O}_4$  on the formation of  $(\text{Bi}_{1.6}\text{Pb}_{0.4})\text{Sr}_2\text{Ca}_2\text{Cu}_3\text{O}_{10}$  and its superconducting properties, and reported that the addition with 0.01 wt.% enhanced both  $T_c$  and  $J_c$ .

The short coherence length of high-temperature superconductors (HTSCs) produces a significant rounding in the

electrical resistivity transition curve [14]. This provides the possibility to study the fluctuations of the superconducting Cooper pairs over an extended temperature region above  $T_c$ . These interesting studies may give information about the microscopic parameters such as the coherence length along  $c$ -axis, cross-over temperature, dimensionality of the order parameter and superconducting parameters such as the lower and upper critical magnetic fields and critical current density [15]. In addition, theoretical concepts of the critical regime close to  $T_c$  or of the Cooper pairs formation may be tested. In HTSCs the fluctuation-induced conductivity was widely investigated on different samples by several groups [16–20], and most of these investigations are based on the Aslamazov–Larkin (AL) model [21].

This work studied the effect of nanosized ferrite  $\text{CoFe}_2\text{O}_4$  on the formation of  $\text{GdBa}_2\text{Cu}_3\text{O}_{7-\delta}$  superconducting phase. Furthermore, the superconducting parameters such as zero-temperature coherence length along  $c$ -axis, lower and upper critical magnetic fields, and  $J_c$  were estimated from excess conductivity analysis.

## 2 Experimental Details

Nanosized ferrite  $\text{CoFe}_2\text{O}_4$  powder was prepared by chemical coprecipitation method. Pure chemical reagents of  $\text{FeCl}_3$  and  $\text{CoCl}_2 \cdot 6\text{H}_2\text{O}$  were first dissolved in bidistilled water, and the Co/Fe molar ratio was fixed to 1/2. An alkaline solution (NaOH) was added to the salt solution till the pH was adjusted to 12.5. The solution was heated with continuous stirring at 60 °C for 2 h. The coprecipitated powder was filtered and washed for several times with bidistilled water and dried in an oven in air atmosphere at 90 °C for 24 h. Finally, the dried powder was calcined in air at 600 °C for 4 h. The nanosized ferrite  $\text{CoFe}_2\text{O}_4$  was characterized by XRD using Shimadzu-7000 powder diffractometer with  $\text{Cu-K}\alpha$  radiation ( $\lambda = 1.54056 \text{ \AA}$ ) in the range  $10^\circ \leq 2\theta \leq 80^\circ$ . The crystallite-size of nanosized  $\text{CoFe}_2\text{O}_4$  was determined using the Williamason–Hall plot equation [7]:  $\beta \cos \theta = 2 \frac{\Delta d}{d} \sin \theta + \frac{0.9\lambda}{D}$ , where  $\beta$  is the full width at half maximum (FWHM) of the broadened diffraction line (in radian),  $D$  is the diameter of the crystallite (in nm),  $\lambda$  is the wavelength of X-rays (in nm),  $\theta$  is the angle of diffraction peak (in degree), and  $(\Delta d/d)$  is the microstrain (fractional change in Bragg's plane spacing). The plot of  $\beta \cos \theta$  with  $\sin \theta$  gave a straight line with slope  $= 2 \frac{\Delta d}{d}$  and intersection with  $y$ -axis  $= \frac{0.9\lambda}{D}$ . Furthermore, the crystallite size of nanosized  $\text{CoFe}_2\text{O}_4$  was also determined using Jeol transmission electron microscope JEM-100CX, operated at 80 kV.

Superconducting samples of type  $(\text{CoFe}_2\text{O}_4)_x\text{GdBa}_2\text{Cu}_3\text{O}_{7-\delta}$ ,  $0.0 \leq x \leq 0.1$  wt.%, were prepared by the conventional solid-state reaction technique. The starting materials  $\text{Gd}_2\text{O}_3$ ,  $\text{BaCO}_3$ , and  $\text{CuO}$  (purity  $\geq 99.9$ ) were crushed

manually in an agate mortar and were sifted using a 125- $\mu\text{m}$  sieve to get a homogeneous mixture. The powder subjected to calcinations process in air at 840 °C and 880 °C for 24 h each. The resulting powder was ground and sifted, and  $x$  wt.% of nanosized ferrite  $\text{CoFe}_2\text{O}_4$  was added to the resulting powder. The mixed powder was pressed in a disc form (1.5 cm in diameter and 0.3 cm in thickness). Discs were sintered in air at 930 °C with a heating rate of 4 °C/min and held at this temperature for 24 h. The samples were cooled by a rate of 1 °C/min to 450 °C and kept at this temperature for 10 h under oxygen flow to control the oxygen-content of the final compounds. Then, they slowly cooled by a rate of 1 °C/min to room temperature.

The prepared samples were characterized by XRD using Shimadzu-7000 powder diffractometer with  $\text{Cu-K}\alpha$  radiation ( $\lambda = 1.54056 \text{ \AA}$ ) in the range  $4^\circ \leq 2\theta \leq 70^\circ$ . The grain morphology of the samples was identified using Jeol scanning electron microscope JSM-5300, operated at 25–30 kV, with a resolution power of 4 nm. Samples of dimensions  $2 \times 2 \times 3 \text{ mm}^3$  were mounted on the SEM stubs and then coated with gold using JEOL JFC-1100 E ion sputtering device. The SEM observations were carried out at magnifications up to 5000 and probe current of the order of 10 mA.

The electrical resistivity of the prepared samples was measured by a conventional four-probe technique from room temperature down to zero-resistivity temperature  $T_0$  with a closed cycle helium cryogenic refrigeration (Displex) system. The samples used for resistivity measurement had dimensions of about  $1.5 \times 0.2 \times 0.3 \text{ cm}^3$ . Copper leads attached to the samples using a conductive silver paint. The temperature of the samples was monitored by a Chromel versus Fe–Au thermocouple and stabilized with the aid of a temperature controller to within  $\pm 0.1 \text{ K}$ . A typical excitation of 1 mA, applied from Keithly 255 current source, was used to avoid heating effects on the samples. The potential drop across the sample was measured using a Keithly 181 digital nanovoltmeter. The voltage was determined by taking the average of the values measured with the normal and the reverse directions of applied current to eliminate the thermoelectric voltages of the junction leads.

## 3 Results and Discussion

XRD pattern of nanosized ferrite  $\text{CoFe}_2\text{O}_4$  is shown in Fig. 1. All the diffraction peaks can be indexed by the face center cubic structure of cobalt ferrite with space group  $\text{Fd}3\text{m}$ . The results indicate that the prepared nanosized  $\text{CoFe}_2\text{O}_4$  ferrite is a high pure phase without any impurities. The crystallite-size determined from the Williamason–Hall plot equation is 8.45 nm. Figure 2 shows the TEM image of the nanosized  $\text{CoFe}_2\text{O}_4$  ferrite. The  $\text{CoFe}_2\text{O}_4$  particles are spherical in shape with diameters within the range of

**Fig. 1** X-ray powder diffraction patterns for nanosized ferrite  $\text{CoFe}_2\text{O}_4$ . The inset shows the variation of  $\beta \cos \theta$  versus  $\sin \theta$

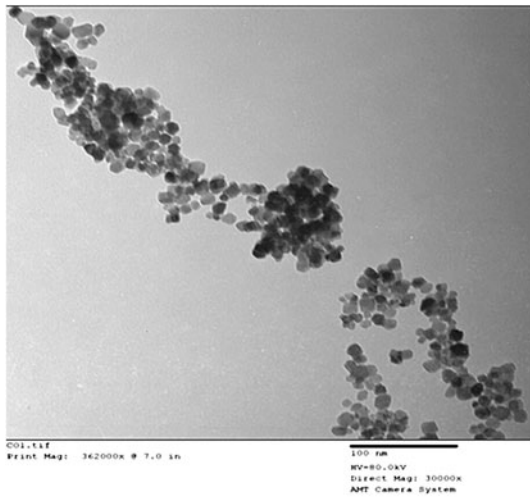
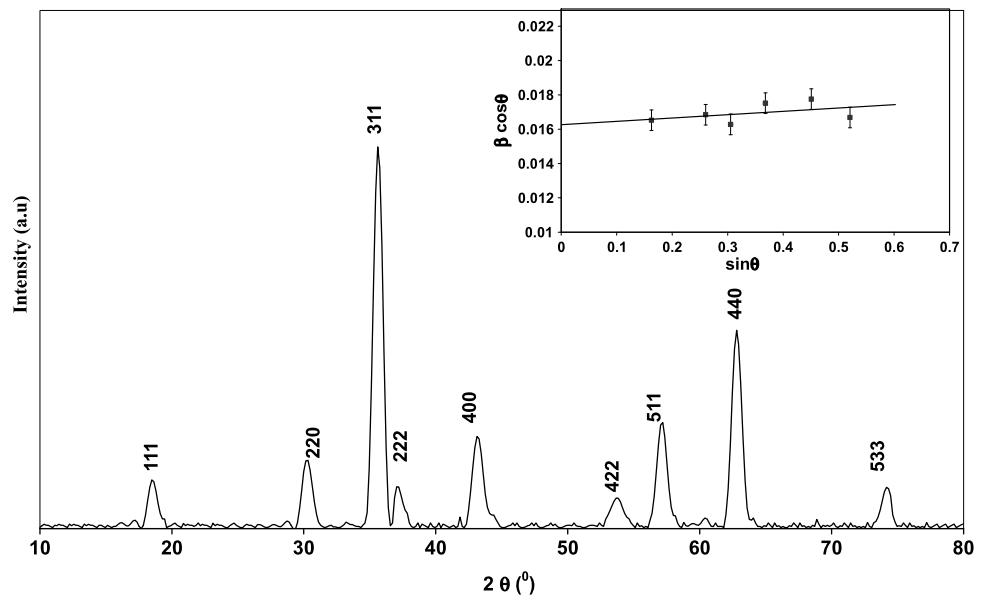


**Fig. 2** TEM image for nanosized ferrite  $\text{CoFe}_2\text{O}_4$

6–8 nm, which is in a good agreement with XRD measurements. Some moderately agglomerated particles as well as separated particles are present in the image. Agglomeration is understood to increase linearly with annealing temperature, and hence some degree of agglomeration at this temperature (600 °C) appears unavoidable.

XRD patterns of  $(\text{CoFe}_2\text{O}_4)_x\text{GdBa}_2\text{Cu}_3\text{O}_{7-\delta}$ , ( $x = 0.0, 0.01, 0.06,$  and  $0.1$  wt.%) are shown in Fig. 3. It is observed that all peaks belong to the main orthorhombic peaks of  $\text{GdBa}_2\text{Cu}_3\text{O}_{7-\delta}$  with a space group  $P_{mmm}$  and an insignificant peak belong to the nonsuperconducting phase  $\text{BaCuO}_2$  [22]. It should be mentioned that there are no peaks corresponding to Co- or Fe-based compounds detected in the XRD patterns for all prepared samples. This result is consistent with that obtained by Wimbush et al.

[13] in YBCO thin film added with ferromagnetic nanosized  $\text{CoFe}_2\text{O}_4$ . The relative volume fraction of Gd-123 and  $\text{BaCuO}_2$  phases is estimated by comparing the intensities of the whole pattern [23], according to the relations

$$[\text{Gd-123}] \% = \frac{\sum I[\text{Gd-123}]}{\sum I[\text{Gd-123}] + \sum I[\text{BaCuO}_2]}, \quad (1)$$

$$[\text{BaCuO}_2] \% = \frac{\sum I[\text{BaCuO}_2]}{\sum I[\text{Gd-123}] + \sum I[\text{BaCuO}_2]}, \quad (2)$$

where  $I$  is the peak intensity of the present phases above the baseline. The calculated values of the volume fraction of  $(\text{CoFe}_2\text{O}_4)_x\text{GdBa}_2\text{Cu}_3\text{O}_{7-\delta}$  are listed in Table 1. The relative volume fraction of Gd-123 phase increases as  $x$  increases from 0.0 to 0.01 wt.%, followed by a decrease in its value with further increase in  $x$ . This behavior confirms the change of the main intensity peak at  $32.68^\circ$  for Gd-123 phase. On the other hand, a little increase in the volume fraction of the impurity phase  $\text{BaCuO}_2$  is observed for  $x > 0.01$  wt.%. This means that higher concentrations of nanosized  $\text{CoFe}_2\text{O}_4$  may lead to changing the reaction rate which slightly retards the Gd-123 phase formation. Indeed, the presence of nanosized  $\text{CoFe}_2\text{O}_4$  ferrite in the transient liquid forming at the reaction temperature can affect the viscosity of the liquid, its homogeneity, and the formation rate of the Gd-123 phase. On the other hand, a second possible explanation is the ability of the higher concentrations of solid nanosized  $\text{CoFe}_2\text{O}_4$  ferrite to prevent the spatial phase growth.

Figures 4(a) and (b) display the SEM micrographs of the fractured surface of  $(\text{CoFe}_2\text{O}_4)_x\text{GdBa}_2\text{Cu}_3\text{O}_{7-\delta}$  ( $x = 0.0$  and  $0.1$  wt.%), respectively. From the surface morphology of nanosized ferrite  $\text{CoFe}_2\text{O}_4$  free sample, the formed grains

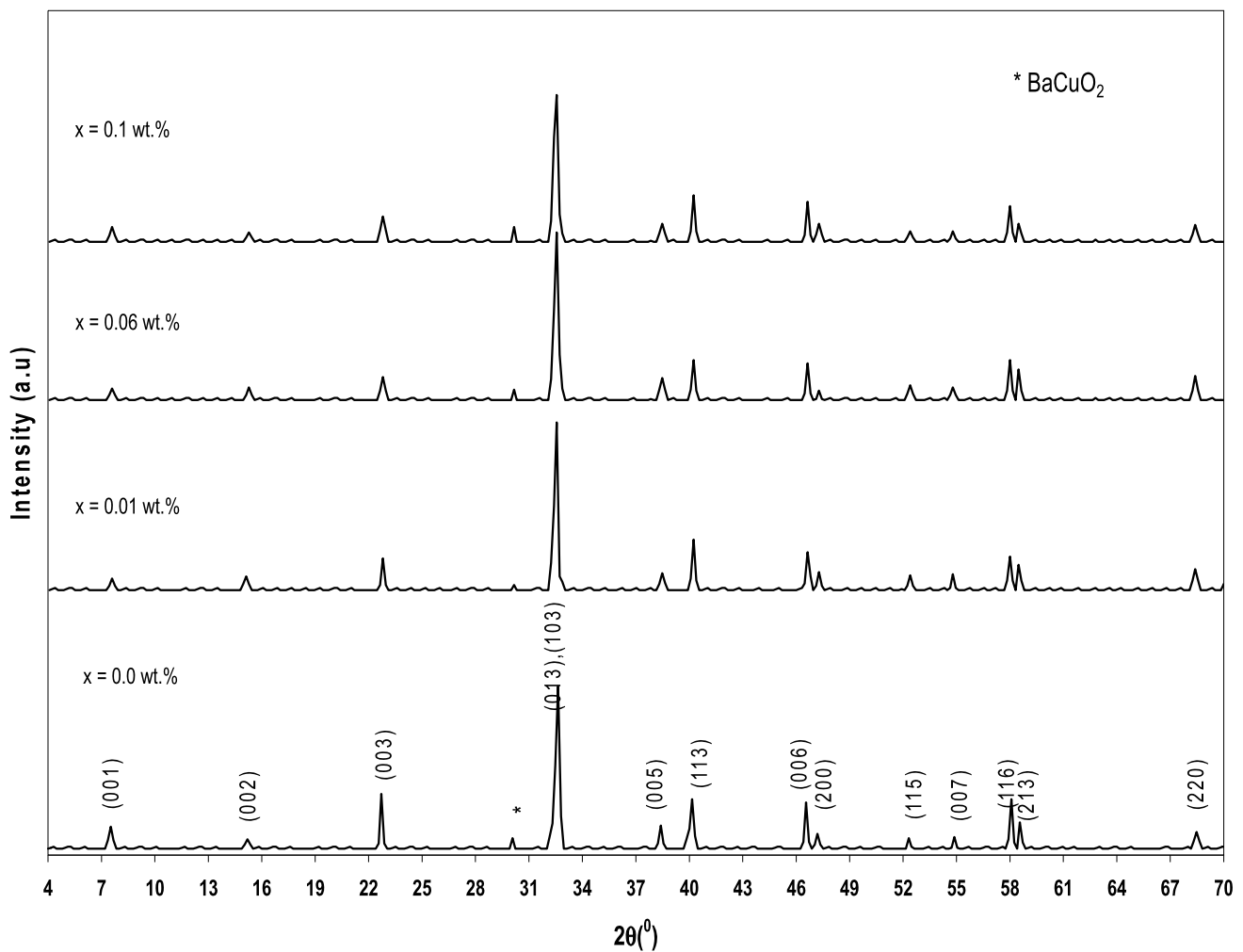


**Fig. 3** X-ray powder diffraction patterns for  $(\text{CoFe}_2\text{O}_4)_x\text{GdBa}_2\text{Cu}_3\text{O}_{7-\delta}$  ( $x = 0.0, 0.01, 0.06,$  and  $0.1$  wt.%)

**Table 1** The variation of the relative volume of Gd-123 and  $\text{BaCuO}_2$  with the content of nanosized ferrite  $\text{CoFe}_2\text{O}_4$ ,  $x$  wt.%

$x$ wt.%	Gd-123 %	$\text{BaCuO}_2$ %
0.0	97.36	2.64
0.01	98.33	1.67
0.02	97.87	2.13
0.04	97.67	2.33
0.06	97.52	2.48
0.08	96.98	3.02
0.1	96.00	4.00

are well connected rectangular-like grains randomly oriented in all directions. A white patches and small white particles in addition to rectangular grains are observed for  $x = 0.1$  wt.%. This may be due to the sticking of nanosized ferrite  $\text{CoFe}_2\text{O}_4$  on the surface of the grains, leading to increase in grain connectivity. Furthermore, randomly

distributed spherical grains are observed, indicating a secondary phase at the formation of  $\text{BaCuO}_2$ . This result supported the decrease of relative volume fraction of Gd-123 at  $x = 0.1$  wt.%.

The temperature dependence of the electrical resistivity for  $(\text{CoFe}_2\text{O}_4)_x\text{GdBa}_2\text{Cu}_3\text{O}_{7-\delta}$  ( $x = 0.0, 0.02, 0.06,$  and  $0.1$  wt.%) are shown in Fig. 5. All samples show a metallic-like behavior in the normal state followed by a superconducting transition to zero resistivity at temperature  $T_0$ . A small curvature above  $T_c$  is observed for all samples, which is a characteristic of superconducting thermodynamic fluctuations. These fluctuations occur at finite temperatures due to the appearance of Cooper pairs above  $T_c$  [24]. The normal-state resistivity  $\rho_n$  is calculated from the fitting of resistivity measurements, in the temperature range from 300 K down to  $2 T_c$ , according to the following relation:

$$\rho_n(T) = \rho_0 + \beta T, \quad (3)$$

where  $\beta$  is the resistivity temperature coefficient, and  $\rho_0$  is the residual resistivity. The values of  $T_c$ ,  $T_0$ ,  $\rho_0$ , and  $\rho_{room}$  for different  $x$  are listed in Table 2. Both  $\rho_{room}$  and  $\rho_0$  decrease as  $x$  increases from 0.0 to 0.01 wt.% and then increase with further increase in  $x$ . The lowest values of  $\rho_{room}$  and  $\rho_0$  indicate that low  $\text{CoFe}_2\text{O}_4$  addition can reduce grain boundaries, improves the quality of the sample, and reduces the defects. The increase in both  $\rho_{room}$  and  $\rho_0$

for  $x > 0.01$  wt.% is probably due to the decrease in relaxation time, resulting from a great number of defects in the final compound. These results are also consistent with those obtained from XRD and SEM data. The decrease in  $T_0$  with  $x$  is attributed to the progressive decoupling of the superconducting grains with microscopic inhomogeneities such as secondary phase, grain boundaries, twin boundaries, and crack incorporated in the bulk. The superconducting transition temperature  $T_c$ , which marks the superconducting transition within the grains and is determined as the temperature corresponding to the crest in  $d\rho/dT$  curve [25]. The derivative  $d\rho/dT$  for  $(\text{CoFe}_2\text{O}_4)_x\text{GdBa}_2\text{Cu}_3\text{O}_{7-\delta}$  ( $x = 0.0, 0.02, 0.06,$  and  $0.1$  wt.%) is shown in the inset of Fig. 5. All the samples show almost a single peak at  $T_c$ , indicating the superconducting transition within the grains. It can be seen that  $T_c$  suppresses form 91.77 K to 79.95 K as  $x$  increases from 0.0 to 0.1 wt.%, consistent with the previous studied for the bulk superconductors material adding with a small amounts of magnetic impurities [26–28].

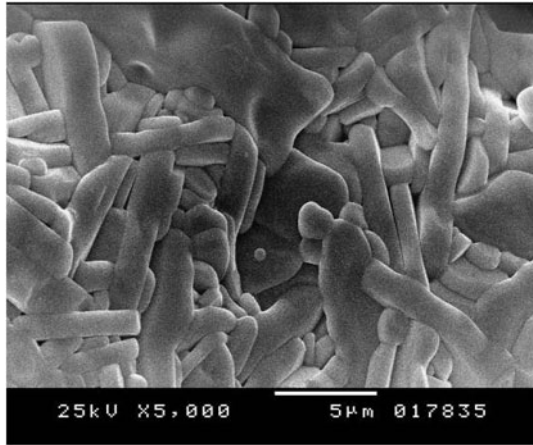
To study the effect of nanosized ferrite  $\text{CoFe}_2\text{O}_4$  on the excess of conductivity above  $T_c$ , the excess conductivity,  $\Delta\sigma$  is defined by

$$\Delta\sigma = \sigma_m(T) - \sigma_n(T) = \frac{1}{\rho_m(T)} - \frac{1}{\rho_n(T)}, \tag{4}$$

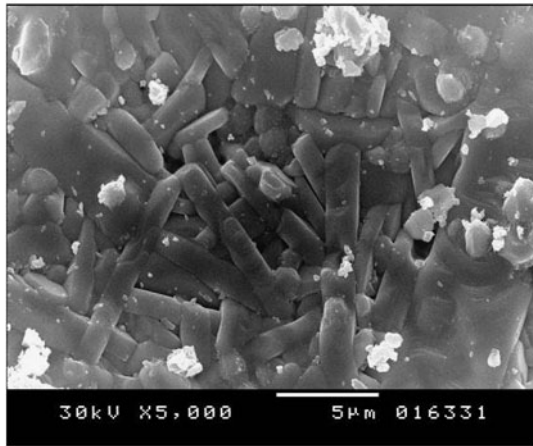
where  $\rho_m(T)$  is the measured resistivity, and  $\rho_n(T)$  is the normal state resistivity determined from Eq. (3). The normalized excess conductivity  $\frac{\Delta\sigma}{\sigma_{room}}$  was calculated by Aslamazov and Larkin [21], using a microscopic approach in the mean field region (MFR), where the fluctuations are small, and it is expressed as

$$\frac{\Delta\sigma}{\sigma_{room}} = At^n, \tag{5}$$

where  $t$  is a reduced temperature,  $t = \frac{T-T_c}{T_c}$ , and  $n$  is the critical exponent which is related to the conduction dimen-



a



b

**Fig. 4** SEM images for  $(\text{CoFe}_2\text{O}_4)_x\text{GdBa}_2\text{Cu}_3\text{O}_{7-\delta}$  with  $x = 0.0$  wt.% (a) and  $0.1$  wt.% (b)

**Table 2** The variations of  $T_c$ ,  $T_0$ ,  $\rho_0$ , and  $\rho_{room}$  for  $(\text{CoFe}_2\text{O}_4)_x\text{GdBa}_2\text{Cu}_3\text{O}_{7-\delta}$ ,  $0.0 \leq x \leq 0.1$  wt.%

$x$ wt.%	$T_c$ (K)	$T_0$ (K)	$\rho_0$ (mΩ cm)	$\rho_{room}$ (mΩ cm)
0.0	91.77	82.25	0.519	1.23
0.01	88.68	80.87	0.507	1.21
0.02	85.15	76.75	0.513	1.25
0.04	83.63	74.00	0.906	1.96
0.06	81.83	71.00	0.908	2.07
0.08	80.50	69.50	0.913	2.66
0.1	79.95	66.62	1.500	3.32

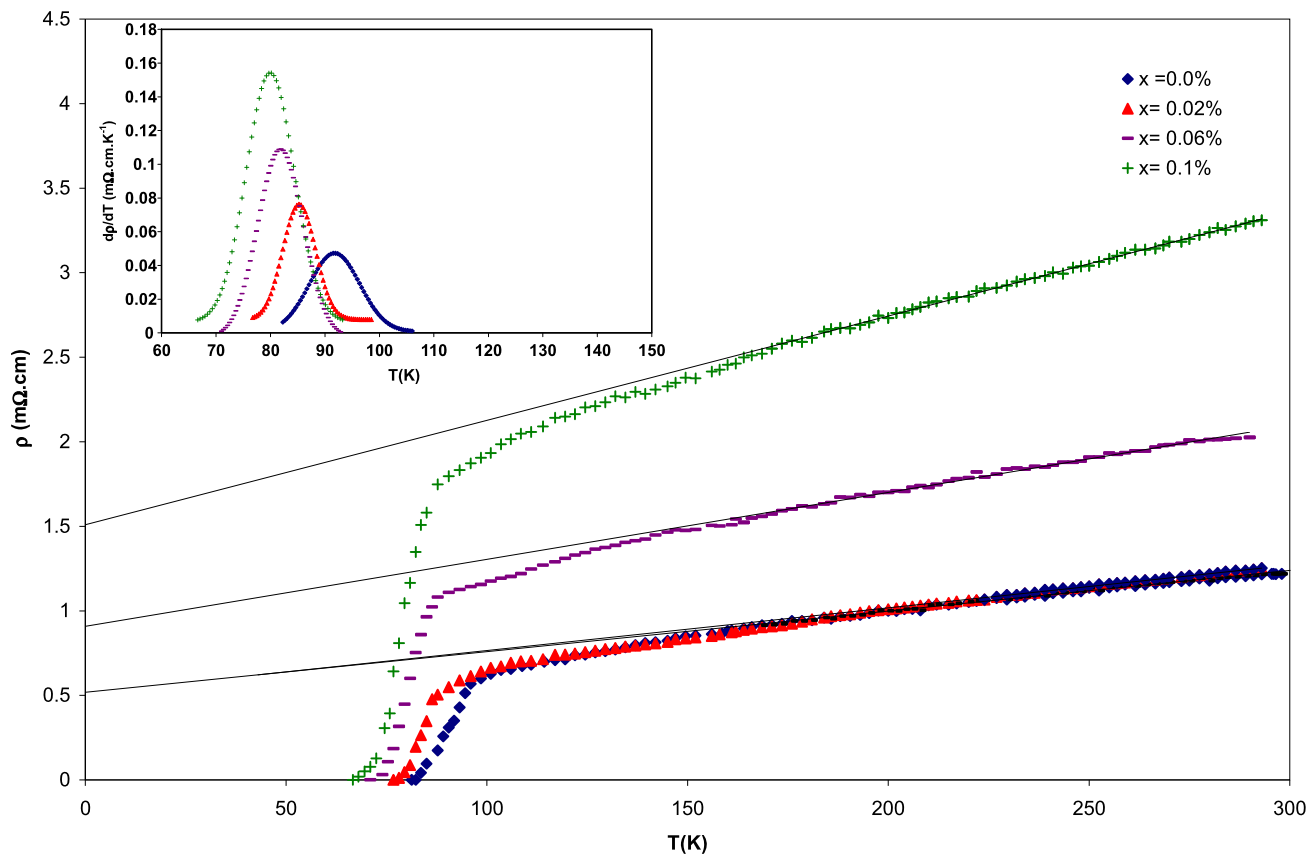


**Fig. 5** Variation of electrical resistivity versus temperature for  $(\text{CoFe}_2\text{O}_4)_x\text{GdBa}_2\text{Cu}_3\text{O}_{7-\delta}$  ( $x = 0.0, 0.02, 0.06,$  and  $0.1$  wt.%), the inset show  $d\rho/dT$  curves versus temperature

sionality as follows [29–31]:

$$n = \begin{cases} -0.3 & \text{for dynamic (cr) fluctuations,} \\ -0.67 & \text{for static (cr) fluctuations,} \\ -0.5 & \text{for 3D fluctuations,} \\ -1.0 & \text{for 2D fluctuations,} \\ -1.5 & \text{for 1D fluctuations,} \\ -3.0 & \text{for sw fluctuations,} \end{cases} \quad (6)$$

and  $A$  is the temperature independent amplitude, given by [32, 33]

$$A = \begin{cases} \frac{e^2}{32\hbar\xi_c(0)\sigma_{\text{room}}} & \text{for a three-dimensional region (3D),} \\ \frac{e^2}{16\hbar d\sigma_{\text{room}}} & \text{for a two-dimensional region (2D),} \end{cases} \quad (7)$$

where  $\xi_c(0)$  is the zero-temperature coherence length along the  $c$ -axis, and  $d$  is the effective layer thickness of the 2D system.

It is seen that the 3D-to-2D crossover is mainly found above  $T_c$  at a particular temperature  $T_{\text{LD}}$ , which is different for different samples [34, 35]. Lawrence and Doniach (LD) introduced the concept of interlayer coupling strength  $J$ , and

in the LD model,  $\Delta\sigma$  is expressed as [36]

$$\Delta\sigma = \left[ \left[ \frac{e^2}{16\hbar d} \right] t^{-1} \left\{ 1 + 2\xi_c(0)/d \right\}^2 \right]^{-1/2}. \quad (8)$$

This expression predicts a behavior of the crossover from 3D to 2D of the order parameter fluctuations at temperature  $T_{\text{LD}}$ :

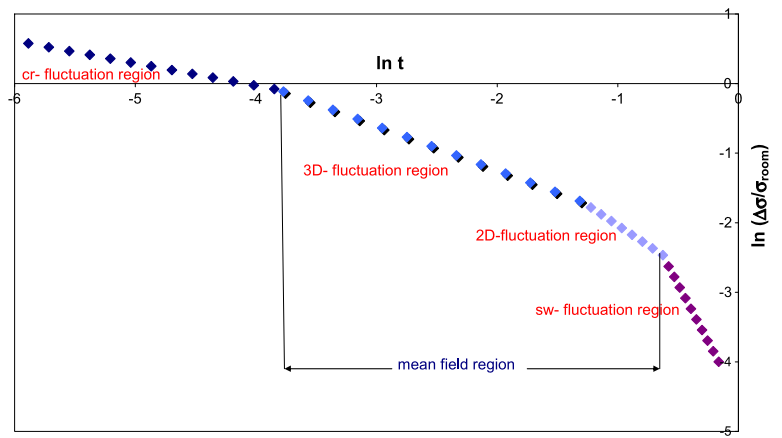
$$T_{\text{LD}} = T_c \left\{ 1 + \left[ 2\xi_c(0)/d \right]^2 \right\}, \quad (9)$$

where  $J = [\xi_c(0)/d]^2$ .

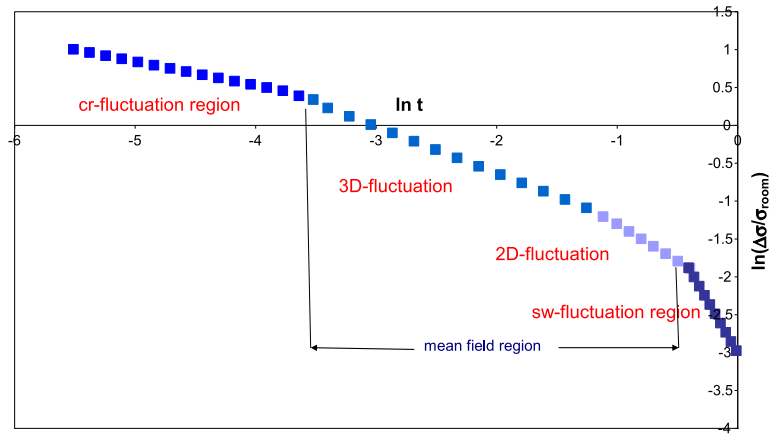
The normalized excess conductivities  $\frac{\Delta\sigma}{\sigma_{\text{room}}}$  as functions of a reduced temperature  $t$ , calculated according to Eq. (5), are plotted as an ln–ln plot for  $(\text{CoFe}_2\text{O}_4)_x\text{GdBa}_2\text{Cu}_3\text{O}_{7-\delta}$ , ( $x = 0.0, 0.01,$  and  $0.06$  wt.%) in Figs. 6a, b, c, respectively.

Evidently, each plot shows four significant different regions. Different regions of the plots are linearly fitted, and the conductivity exponent  $n$ -values are determined from the slopes and listed in Table 3. The first region lies at a temperature much higher than the mean field temperature ( $T_{\text{mf}}$ ), meaning that the GL theory breaks down and short wave fluctuations play a dominant role [37]. In this temperature range, the normalized excess conductivity decreases sharply with  $n(\text{sw}) \approx -3$ , which is in good agreement with the theoretical prediction. However, this behavior was attributed

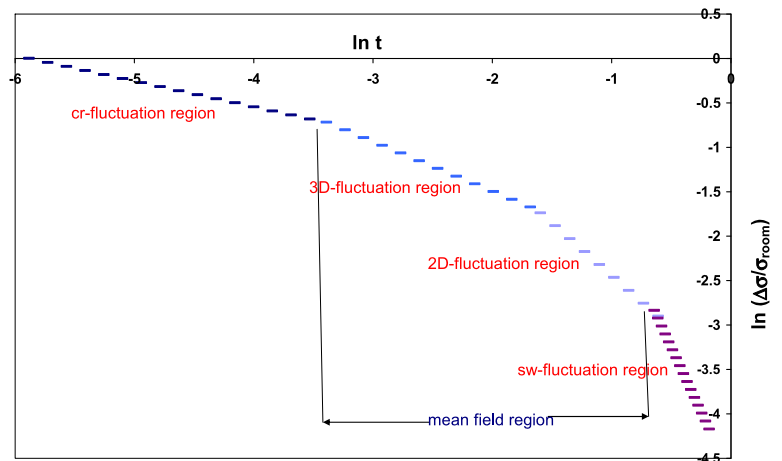
**Fig. 6** The variation of the normalized excess conductivity  $\frac{\Delta\sigma}{\sigma_{room}}$  with the reduced temperature  $t$  in ln–ln plot for  $(CoFe_2O_4)_xGdBa_2Cu_3O_{7-\delta}$  with  $x = 0.0$  wt.% (a), 0.01 wt.% (b), and 0.06 wt.% (c)



(a)



(b)



(c)

to the change in the carrier density or the band structural changes in the Fermi surface, where both of them have a major impact on the change in the order parameter. Since there is a change in the room temperature resistivity,  $T_c$  and hence may be the oxygen content for the present samples, the band structural change in the Fermi surface may

be responsible for shortwave fluctuation behavior [38]. It is believed that the width of this region is controlled by created oxygen vacancies either in Cu–O<sub>2</sub> planes or in Cu–O chains [20]. With decreasing temperature, a crossover between shortwave fluctuations and mean field region is observed at a temperature  $T^{2D-sw}$ . The mean field region con-

**Table 3** The variation of conductivity exponents and the cross-over temperatures for  $(\text{CoFe}_2\text{O}_4)_x\text{GdBa}_2\text{Cu}_3\text{O}_{7-\delta}$  with different  $x$ 

$x$ wt. %	$n$ (cr)	$n$ (3D)	$n$ (2D)	$n$ (sw)	$T^{\text{cr-3D}} = T_G$ (K)	$T^{3\text{D-2D}} = T_{\text{LD}}$ (K)	$T^{2\text{D-sw}}$ (K)
0.0	-0.32	-0.64	-1.15	-3.30	93.89	118.88	143.68
0.01	-0.31	-0.61	-0.97	-2.77	91.13	118.05	142.43
0.02	-0.31	-0.65	-0.92	-3.00	89.61	106.75	140.28
0.04	-0.31	-0.49	-0.88	-2.85	86.16	104.88	132.86
0.06	-0.29	-0.56	-1.18	-2.77	84.22	98.51	126.28
0.08	-0.33	-0.45	-1.01	-3.17	82.61	85.75	122.40
0.1	-0.34	-0.61	-0.96	-2.95	82.34	84.62	113.78

sists of two distinct linear parts. In the first part at temperature above  $T_{\text{LD}}$ , the conductivity exponent values  $n$  (2D) vary from  $-0.88$  to  $-1.18$ , indicating the existence of 2D fluctuations, whilst at temperature below  $T_{\text{LD}}$ , the conductivity exponent values  $n$  (3D) vary from  $-0.45$  to  $-0.65$ , reflecting the appearance of 3D fluctuations. The 3D–2D crossover temperatures  $T^{3\text{D-2D}} = T_{\text{LD}}$  are calculated from the intersection of the two linear parts, and these values are listed in Table 3. The 3D–2D crossover could be attributed to the highly anisotropy of high-temperature superconductors. In (2D) region, the charge-carriers show some ability to move along the molecular planes in the material, whereas in 3D, the charge carriers may move between the molecular planes, and they are more affected by the thermal fluctuations than that in the 2D region. This means that the charge-carriers tend to move more freely in the whole sample before they make Copper pairs, above  $T_c$ . Finally, at Ginzburg temperature ( $T_G$ ), a crossover between three-dimensional fluctuations and critical fluctuations are occurred. In the critical region, below  $T_G$ , the fluctuations in the order parameter become of the same magnitude as the order parameter itself [31], and the GL theory becomes unsuitable. In this region, the conductivity exponent values  $n$  (cr) vary from  $-0.29$  to  $-0.34 \approx -0.3$ . These values are expected from the 3D-XY universality class, with dynamics given by the representative E-model [39]. This model based on the coupling of a two-dimensional superconducting order parameter with asymmetry-breaking field (SBF). It can be seen that  $T_{\text{LD}}$  shifted to a lower values with nanosized  $\text{CoFe}_2\text{O}_4$  addition. This means that a sizable fraction of nanosized  $\text{CoFe}_2\text{O}_4$  resides inside the grains, which could be affected by  $T_{\text{LD}}$ .  $T_{\text{LD}}$  is a sensitive parameter to the electronic structure in the normal state [40] and can strongly influence by the content of nanosized  $\text{CoFe}_2\text{O}_4$ .

The thermodynamic critical field  $B_c(0)$  is related to the Ginzburg number  $N_G$  according to the following equation [41]:

$$N_G = \left| \frac{T_G - T_c}{T_c} \right| = \frac{1}{2} \left( \frac{k_B}{B_c^2(0) \gamma^2 \xi_c^3(0)} \right)^2, \quad (10)$$

where  $\gamma = \frac{\xi_{ab}}{\xi_c}$  is the anisotropy parameter (from 5 to 8 for Y-123 depending on oxygen content [42]). The Ginzburg number  $N_G$  is obtained using Eq. (10) and assuming that the 3D Gaussian regime delimits the validity of the Ginzburg–Landau theory [43]. Knowing  $B_c(0)$ , the penetration depth  $\lambda(0)$ , the lower critical magnetic field  $B_{c1}(0)$ , the upper critical magnetic field  $B_{c2}(0)$ , and the critical current density  $J_c(0)$  can be calculated using the GL relations [44]:

$$B_c = \frac{\Phi_0}{2\sqrt{2}\pi\lambda(0)\xi_c(0)}, \quad (11)$$

$$B_{c1} = \frac{B_c}{k\sqrt{2}} \ln k, \quad (12)$$

$$B_{c2} = \sqrt{2}k B_c, \quad (13)$$

$$J_c = \frac{4k B_{c1}}{3\sqrt{3}\lambda(0) \ln k}, \quad (14)$$

where  $\Phi_0 = \frac{h}{2e}$  is the flux-quantum number, and  $k = \frac{\lambda(0)}{\xi_c(0)}$  is the Ginzburg–Landau parameter. The calculated superconducting parameters for the samples under investigations are listed in Table 4. It is clear that the zero-temperature coherence length along the  $c$ -axis decreases as  $x$  increase from 0.0 to 0.01 wt.% and then increases for  $x > 0.01$  wt.%, but their values are longer than that for Gd-123 thin film ( $\xi_c(0) = 3$  Å) [45] and for Y-123 single crystal ( $\xi_c(0) = 1.1$  Å) [46]. These results can be explained according to the simple grain model. Ceramic samples exhibit complex transport behavior because they are composed of crystallites, where the transport depends on the mixing of the conductor planes ( $ab$ ) with the insulating  $c$ -axis, on the inhomogeneities and the nature of present defects, and on the crystalline boundaries. The observed decrease of the coherence length over several electronic layers along the  $c$ -axis, for  $x = 0.01$  wt.%, gives rise to decrease coherence volume containing Cooper pairs formed at higher temperatures and results in decrease of the  $T_c$ . Actually, the R-123 systems are three-dimensional (3D) with two Cu–O<sub>2</sub> planes and one Cu–O chain. The coupling between planes and chains plays a major role in superconductivity of these materials. Therefore, the interlayer cou-



**Table 4** The variation of the calculated superconducting parameters for  $(\text{CoFe}_2\text{O}_4)_x\text{GdBa}_2\text{Cu}_3\text{O}_{7-\delta}$  with different  $x$ 

$x$ wt.%	$\xi_c(0)$ (Å)	$d$ (Å)	$J$	$B_c(0)$ (T)	$\lambda$ (Å)	$k$	$B_{c1}$ (T)	$B_{c2}$ (T)	$J_c \times 10^4$ (A/cm <sup>2</sup> )
0.0	11.90	45.14	0.07	24.39	80.11	6.73	4.88	232.32	16.58
0.01	5.85	17.82	0.11	67.47	58.92	10.06	10.94	960.48	62.34
0.02	5.90	17.16	0.12	54.76	72.05	12.21	7.93	946.14	41.37
0.04	9.67	32.25	0.09	31.14	77.27	7.99	5.73	351.8	21.94
0.06	21.41	117.35	0.03	9.52	114.1	5.33	2.11	71.77	4.54
0.08	27.14	274.28	0.01	6.86	124.9	4.60	1.61	44.68	2.99
0.1	27.85	142.57	0.04	6.39	130.7	4.70	1.49	42.44	2.66

pling of these materials is larger as compared to those of the TBCCO systems [15, 17, 24], and consequently the degree of anisotropy ( $\rho_c/\rho_{ab}$ ) becomes lower. The critical magnetic fields ( $B_c$ ,  $B_{c1}$ , and  $B_{c2}$ ) and the critical current density  $J_c$  are enhanced up to 0.01 wt.%, and then they suppress with a further increase in  $x$ . The increase in thermodynamic parameters for  $x = 0.01$  wt.% could be due to the reduction of magnetic vortex motion via improvement of pinning capability within the sample, suggesting the presence of strong pinning sources. These results are consistent with those obtained by Bouchoucha et al. [47] for Y-123 phase added with nanosized  $\text{Zn}_{0.95}\text{Mn}_{0.05}\text{O}$  and  $\text{ZnO}$ . For  $x > 0.01$  wt.%, the decrease of  $J_c$  is due to the cancellation of supercurrents by the ferromagnetic nanosized ferrite  $\text{CoFe}_2\text{O}_4$  [26].

#### 4 Conclusion

Nanosized  $\text{CoFe}_2\text{O}_4$  ferrite has been successfully prepared via coprecipitation method with average crystallite size 6–8 nm. The effect of addition nanosized  $\text{CoFe}_2\text{O}_4$  ferrite on the phase formation of Gd-123 phase has been studied, and we found that the volume fraction increased as  $x$  increased from 0.0 to 0.01 wt.%. A reduction in  $T_c$  was observed as  $x$  increased from 0.0 to 0.1 wt., consisting with the results of adding magnetic nanosized particles to HTSCs. The analysis of excess conductivity for  $(\text{CoFe}_2\text{O}_4)_x\text{GdBa}_2\text{Cu}_3\text{O}_{7-\delta}$  ( $x = 0.0, 0.01, 0.02, 0.04, 0.06, 0.08, \text{ and } 0.1$  wt.%) revealed the appearance of four fluctuation regions close to and above  $T_c$ . The calculated zero-temperature coherence length along the  $c$ -axis decreased as  $x$  increased from 0.0 to 0.01 wt.%, and then it increased for  $x > 0.01$  wt.%. The critical magnetic fields ( $B_c$ ,  $B_{c1}$ , and  $B_{c2}$ ) and the critical current density  $J_c$  enhanced with  $x$  up to 0.01 wt.%, and then they suppressed with a further increase in  $x$ . These results can be attributed to the improvement of pinning capability within the sample and suggested the presence of pinning sources generated by the suitable small amount of nanosized ferrite  $\text{CoFe}_2\text{O}_4$  addition.

**Acknowledgements** This work was performed in the superconductivity and metallic-glass lab, Physics Department, Faculty of Science, Alexandria University, Alexandria, Egypt.

#### References

- Mochida, T., Chikumoto, N., Murakami, M.: Phys. Rev. B **62**, 1350 (2000)
- Muralidhar, M., Jirsa, M., Sakai, N., Murakami, M., Hirabayashi, I.: Mater. Sci. Eng. B **151**, 90 (2008)
- Hinai, H., Nariki, S., Seo, S.J., Sakai, N., Murakami, M., Otsuka, M.: Supercond. Sci. Technol. **13**, 676 (2000)
- Nariki, S., Sakai, N., Murakami, M.: Supercond. Sci. Technol. **18**, S126 (2005)
- Harada, T., Yoshida, K.: Physica C **383**, 48 (2002)
- Abou-Aly, A.I., Abdel Gawad, M.M.H., Awad, R., G-Eldeen, I.: J. Supercond. Nov. Magn. **24**, 2077 (2011)
- Elokr, M.M., Awad, R., Abd El-Ghany, A., Abou Shama, A., Abd El-wanis, A.: J. Supercond. Nov. Magn. **24**, 1345 (2011)
- Mohammed, N.H., Abou-Aly, A.I., Ibrahim, I.H., Awad, R., Rebab, M.: J. Supercond. Nov. Magn. **24**, 1463 (2011)
- Xu, C., Hu, A., Ichihara, M., Sakai, N., Hirabayashi, I., Izumi, M.: Physica C **460–462**, 1341 (2007)
- Xu, C., Hu, A., Sakai, N., Izumi, M., Hirabayashi, I.: Physica C **445–448**, 357 (2006)
- Xu, Y., Hu, A., Xu, C., Sakai, N., Hirabayashi, I., Izumi, M.: Physica C **468**, 1363 (2008)
- Wimbush, S.C., Yu, R., Bali, R., Durrell, J.H., MacManus-Driscoll, J.L.: Physica C **470**, S223 (2010)
- Kong, W., Abd-Shukor, R.: J. Supercond. Nov. Magn. **23**, 257 (2010)
- Irfan, M., Khan, S., Hassan, N., Khan, N.A.: J. Supercond. Nov. Magn. **22**, 769 (2009)
- Abou-Aly, A.I., Ibrahim, I.H., Awad, R., El-Harizy, A., Khalaf, A.: J. Supercond. Nov. Magn. **23**, 1325 (2010)
- Mohanta, A., Behera, D.: Physica C **470**, 295 (2010)
- Abou-Aly, A.I., Awad, R., Ibrahim, I.H., Abdeen, W.: Solid State Commun. **149**, 281 (2009)
- Esmaili, A., Sedghi, H., Amniat-Talab, M., Talebian, M.: Eur. Phys. J. B **79**, 443 (2011)
- Khan, N.A., Khurram, A.A., Firdous, U., Ullah, S., Khan, S.: Physica C **474**, 29 (2012)
- Sedky, A.: J. Low Temp. Phys. **148**, 53 (2007)
- Aslamazov, L.G., Larkin, I.A.: Phys. Lett. A **26**, 238 (1968)
- Nazarova, E.K., Nenkov, K., Fuchs, G., Müller, K.-H.: Physica C **436**, 25 (2006)
- Chen, J.C., Xu, Y., Wu, M.K., Guan, W.: Phys. Rev. B **53**, 5839 (1996)

24. Abou-Aly, A.I., Awad, R., Kamal, M., Anas, M.: *J. Low Temp. Phys.* **163**, 184 (2011)
25. Salamati, H., Kameli, P.: *Solid State Commun.* **125**, 407 (2003)
26. Wang, X.L., Horvat, J., Gu, G.D., Uprety, K.K., Liu, H.K., Dou, S.X.: *Physica C* **337**, 221 (2000)
27. Xu, Y., Izumi, M., Tsuzuki, K., Zhang, Y., Xu, C., Murakami, M., Sakai, N., Hirabayashi, I.: *Supercond. Sci. Technol.* **22**, 095009 (2009) (6 pp.)
28. Xu, Y., Izumi, M., Zhang, Y.F., Kimura, Y.: *Physica C* **469**, 1215 (2009)
29. Han, S.H., Axnäs, J., Zhao, B.R., Rapp, Ö.: *Physica C* **408–410**, 679 (2004)
30. Saleh, S.A., Ahmed, S.A., Elsheikh, E.M.M.: *J. Supercond. Nov. Magn.* **21**, 187 (2008)
31. Lobb, C.J.: *Phys. Rev. B* **36**, 3930 (1987)
32. Pradhan, K., Roy, S.B., Chaddha, P., Chen, C., Wanklyn, B.M.: *Phys. Rev. B* **50**, 7180 (1994)
33. Sharifi, F., Herzog, A.V., Dynes, R.C.: *Phys. Rev. Lett.* **71**, 428 (1993)
34. Ghosh, A.K., Bandyopadhyay, S.K., Basu, A.N.: *J. Appl. Phys.* **86**, 3247 (1999)
35. Konsin, P., Sorkin, B., Ausloos, M.: *Supercond. Sci. Technol.* **11**, 1 (1998)
36. Lawrence, J., Doniach, S., In: Kanda, E. (ed.) *Proc. 12th Conf. Low-Temp Phys.* Kyoto, Tokyo, Keigaku, p. 361 (1970)
37. Reggiani, L., Vaglio, R., Varlamo, A.A.: *Phys. Rev. B* **44**, 9541 (1991)
38. Ghosh, A.K., Basu, A.N.: *Phys. Rev. B* **59**(17), 11193 (1999)
39. Hohenberg, P.C., Halperin, B.I.: *Rev. Mod. Phys.* **49**, 435 (1977)
40. Mohanta, A., Behera, D.: *Physica B* **406**, 877 (2011)
41. Petrovie, A., Fasano, Y., Lortz, R., Decrouc, M., Potel, M., Chevrel, R., Fischer, O.: *Physica C* **460–462**, 702 (2007)
42. Lundqvist, B., Rapp, Ö., Andersson, M.: *Phys. Rev. B* **62**, 3542 (2000)
43. Rojas Sarmiento, M.P., Uribe Laverde, M.A., Vera López, E., Landineza, D.A., Roa-Rojas, J.: *Physica B* **398**, 360 (2007)
44. Poole, P.C., Farach, A.H., Creswick, J.R., Prozorov, R.: *Superconductivity*, 2nd edn. Academic Press/Elsevier, San Diego (2007)
45. Lang, W., Bittner, R., Gehringer, P., Pedarnig, J.D., Bauerle, D.: *Physica B* **284–288**, 993 (2000)
46. Costa, R.M., Pureur, P., Gusmão, M., Senoussi, S., Behnia, K.: *Solid State Commun.* **113**, 23 (2000)
47. Bouchoucha, I., Ben Azzouz, F., Ben Salem, M.: *J. Supercond. Nov. Magn.* **24**, 345 (2011)